ACS APPLIED MATERIALS & INTERFACES

Research Article

www.acsami.org

Biotemplated Syntheses of Macroporous Materials for Bone Tissue Engineering Scaffolds and Experiments in Vitro and Vivo

Xing Li,*[,†] Yayun Zhao,[†] Yue Bing,[†] Yaping Li,[‡] Ning Gan,[†] Zhiyong Guo,[†] Zhaoxiang Peng,[§] and Yabin Zhu[†]

[†]Faculty of Materials Science and Chemical Engineering, Ningbo University, Ningbo 315211, P.R. China

[‡]Department of Orthopaedic Surgery, Affiliated Hospital of School of Medicine, Ningbo University, Ningbo 315211, P.R. China

[§]Department of Orthopedic Surgery, Ningbo Medical Treatment Center Lihuili Hospital, Ningbo 315040, P.R. China

Supporting Information

ABSTRACT: The macroporous materials were prepared from the transformation of cuttlebone as biotemplates under hydrothermal reactions and characterized by Fourier transform infrared spectroscopy (FTIR), X-ray diffraction (XRD), thermogravimetric/differential thermal analyses (TG-DTA), and scanning electron microscopy (SEM). Cell experimental results showed that the prepared materials as bone tissue engineering scaffolds or fillers had fine biocompatibility suitable for adhesion and proliferation of the hMSCs (human marrow mesenchymal stem cells). Histological analyses were carried out by implanting the scaffolds into a rabbit femur, where the bioresorption, degradation, and biological activity of the scaffolds were observed in the animal body. The prepared scaffolds kept the original three-dimensional frameworks with the ordered porous structures, which made for blood circulation, nutrition supply, and the cells implantation. The biotemplated syntheses could provide a new effective approach to prepare the bone tissue engineering scaffold materials.

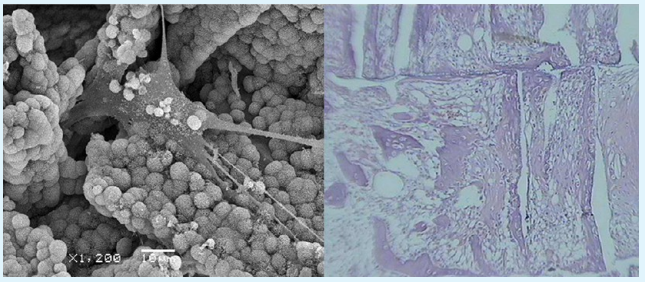

KEYWORDS: *hydroxyapatites, scaffolds, cuttlebones, hydrothermal, macroporous materials, biocompatibility*

1. INTRODUCTION

Design and synthesis of new porous scaffold materials for bone rehabilitation are of great significance since large quantities of skeletal reconstructive surgical cases need to be performed with the scaffold materials each year worldwide.[1,2] In bone healing occurrence, the graft materials play the crucial roles.[3−5] The autologous bones, as the gold-standard of the graft materials, can provide the scaffolds and active factors for bone ingrowth.[6,7] However, aside from the source of the autologous bone being greatly limited, the autologous bone grafts are associated with an 8−39% risk of complications, e.g., hematoma, additional injury, superinfection, surgical complication, postoperative pain, and chronic pain at the donor sites.[8−10] Therefore, autologous bone grafts are normally not recommended for elderly or pediatric patients or for patients with malignant or infectious disease. Alternative strategies, like allo- or xeno-transplantations, have major biocompatibility disadvantages compared with autografts.[11,12] To overcome these limitations, the bone graft substitutes have been used to reconstruct bone defects.[13,14] The perfect bone substitutes are osteoinductive, osteoconductive, biocompatible, and bioresorbable, which should induce minimal or no grafts rejection and can undergo remodeling and support new bone formation. On the other hand, it should be cost-effective and available in the amount required. The bone substitutes as scaffolds are in favor of the bone cells migration, proliferation, and new bone formation.[15] Acellular materials are absorbable fillers that will disappear over time, and scaffold apertures provide room for bone growth into the construction.[16] Calcium phosphate-based ceramics are currently available and widely used in trauma and orthopedic surgery for bone substitutes due to their chemical similarity to bone mineral with minimal immunologic reactions, no foreign body reactions, or no systemic toxicity. Hydroxyapatite (HA, $Ca_5(PO_4)_3(OH)$) and beta tricalciumphosphate (β-TCP, $Ca_3(PO_4)_2$) are well-known bioceramics that possess high tissue compatibility and osteoconductivity.[17,18] However, HA seems to be too stable in vivo because it shows a similar crystalline phase as bone mineral, which would be hard to tend toward chemical and biological equilibrium with bone tissue.[19,20] β-TCP has greater extent dissolution and degradation than HA, and the degradation rate of β-TCP is too fast for optimum bonding to bone (3−10 times faster than HA).[21] To solve the problems above, bi- or multiphase bioceramic materials are preferable as the bone substitutes with a desired surface topography, pore size, channel direction, and trabecular orientation by various techniques.

Received: March 1, 2013
Accepted: June 6, 2013
Published: June 6, 2013

   dx.doi.org/10.1021/am400779e | *ACS Appl. Mater. Interfaces* 2013, 5, 5557−5562

Herein, we used the hydrothermal method to finish the conversion of most $CaCO_3$ in cuttlebone into calcium phosphate composites (HA and/or TCP) for experiments in vitro and vivo, in which the cuttlebone as a porous biotemplate consists of aragonite crystalline calcium carbonate, a small amount of calcium phosphates, and organic matter.[22,23] The prepared materials comprise calcium phosphates with a small amount of calcium carbonates, which are confirmed by thermogravimetry (TG), Fourier transform infrared spectroscopy (FTIR), and X-ray diffraction (XRD). The complex phase composition is favorable to the realization of the balance between absorption and degradation of bioceramic materials. The transformed scaffold materials keep the original ordered natural framework with high porosity rate (85−90%) and large aperture (0.20 × 0.09 mm), which were implanted in the rabbit femur and shown the perfected performance of the material as the bone substitutes.

2. EXPERIMENTAL SECTION

Materials and Instruments. Dulbecco's modified eagle medium (DMEM) substrate (Eurobio), fetal calf serum (Eurobio), trypsin (Eurobio), dimethylsulfoxide (DMSO; Hyclone), green streptomycin (Hyclone), vitamin C (Sigma), dexamethasone (Sigma), 3-(4,5-dimethylthiazol-2-yl)-2,5-diphenyl tetrazolium bromide (MTT, Sigma), alkaline phosphatase staining kit (Sigma), β-glycerol phosphate (Sigma), and high-density polyethylene film (Thermanoxm, United States) were commercially available and used without further purification. The phosphate buffer solution (PBS) was prepared in our laboratory. Other reagents (ethylenediaminetetraacetic acid (EDTA), NaCl, $CaCl_2$, KCl, $Na_2HPO_4{\cdot}H_2O$, analytical-grade) were purchased from Shanghai Biotechnology Ltd. A cell incubator (GBB16, Heraeus, Germany), a fluorescence inverse microscope (Olympus IX71, Japan), IR (FTIR-8900), thermogravimetric/differential thermal analyses (TG-DTA; Exstra 6300II), SEM (Hitachi S-4100), and XRD (a Bruker D8) were used. The 293-cells were kindly provided by Dr. J. R. Lou (School of Medicine, Washington University, USA). Adv-GFP (Adenovirus with Green Luminescence Protein) was obtained from College of Life Sciences (Nanjing Normal University, P.R.China). hMScs were obtained from allogeneic bone marrow transplantations of healthy adult donors after informed consent (Department of Orthopedics, Ninth People's Hospital, Shanghai Jiaotong University School of Medicine, P.R.China).

Preparation of the Scaffold Materials. Cuttlebones (CB, 100 g, 30 × 10 × 3.5 cm) from the sampan-like spine of cuttlefishes were cut into different dimensional cylinders (diameter × height: 5 × 10 mm and 10 × 20 mm, Figure S1, Supporting Information) by a trepan. The mixture of pieces of dry cuttlebone and $(NH_4)_2HPO_4$ (mol/mol, 1:1.1) in aqueous solution were sealed in a 100 mL stainless steel autoclave with Teflon liner and placed in a temperature-controlled electric furnace at 180 °C (heating and cooling rates were 10 $K{\cdot}min^{-1}$). Different times of hydrothermal reaction were tested between 3 and 48 h in independent experiments. The pH of the solution was 7.8−8.2 before being placed in autoclaves and slightly lower after the hydrothermal reaction.

In Vitro Hemocompatibility Measurement. Full human blood was collected with anticoagulant and stored at 4 °C before use. The experiments were finished within 12 h after the blood donation.[24] The hemocompatibility of the scaffold was evaluated by measuring the activated partial thromboplastin time (APTT), prothrombin time (PT), and thrombin time (TT). In brief, platelet poor plasma (PPP) was prepared by centrifuging fresh human blood for 15 min. In a silanized beaker, 2 mL of PPP was added to each sample, and then, the samples were incubated at 37 °C for 10 min. To measure the APTT, a mixture of 200 μL of PPP and 100 μL of APTT reagents was incubated at 37 °C for 3 min. Subsequently, 100 μL of $CaCl_2$ aqueous solution (0.03 M) was added, meanwhile the clotting time was recorded by an automated blood coagulation analyzer (Amelung KC4A, Sigma Diagnostics). The PT and TT experiments were performed by adding 100 μL of PT or TT reagent to 200 μL of PPP in test tubes and then analyzed in the same way. Each experiment was repeated 3 times to give an average value.[24,25]

MTT Assay. According to the international standard ISO10993.5, the toxicological properties of the scaffolds were evaluated by MTT test, and the cell viability was determined as a cytotoxicity parameter.[26] MTT (1.0 mg/mL) was added to the cells and allowed to incubate for 4 h at 37 °C in the CO_2 incubator. The cytotoxicity test was carried out while the cells were in a phase of exponential growth for 48 h, and starting cell density in a 96-well microplate was 5×10^3/well. All negative controls were high density polyethylene film extracts, and positive controls were a series of phenol dilute solution and medium (shown in Table S1, Supporting Information). The initial concentration of the phenol was 6.4 mg/mL. A detailed description of the MTT test was given elsewhere.[27]

Cell-293 Passage. The original culture medium of cell-293 in the 100 mm Petri dish was removed by suction tubes, washed with PBS (10 mL), and digested at 37 °C for 5 min by addition of 0.05% trypsin solution (2 mL), and then, 4 mL of fresh substrate containing a fetal bovine serum was added for stopping digestion. The cell suspension was distributed to new culture dishes with fresh substrates (10 mL/well). When the cytogamy reached more than 80%, the cell suspension was collected and used for subsequent experiments.

Cell-293 Proliferation. Original liquids of Adv-GFP were diluted by the ratio of 19:1 with fresh substrates. After removing the original culture medium of the cell-293, the diluted virus liquids (10 mL) were added to every dish to proliferate for 5 days, and then, the cell-293 suspension was collected. The cell-293 was collected three times through alternately heating at 37 °C and freezing at −80 °C (frozen over 6 h one time).

hMSCs (Human Marrow Mesenchymal Stem Cells) Labeled by Adv-GFP. The virus liquids of Adv-GFP (2 mL) were added into the 80−90% cytogamy MSC cultivated in the Petri dish (multiplicity of infection, MOI = 150). After the virus infected for 16 h, the virus liquids were removed from Petri dish and washed once with PBS, and the original medium was replaced by a fresh one. Then, the effect of GFP gene transfection into hMSCs was observed under a fluorescent inverted microscope excited by blue fluorescence.

In Vitro Adhesion of Adv-GFP-Labeled hMSCs. After being fumigated by ethylene oxide for 24 h, the scaffold materials transferred from the hydrothermal reaction were placed in a 24-well plate, in which cells of hMSC transfected by GFP genes (Adv-GFP-labeled hMSCs) were seeded every well with 1.5 mL (105 cells/mL) and cultured for 12 and 72 h, respectively, and then, nonaherent cells were removed by washing with PBS.

3. RESULTS AND DISCUSSION

Fourier Transform Infrared Spectroscopy (FTIR). Infrared spectroscopy of the sample was measured by using KBr tablets on a Shimadzu FTIR-8900 infrared spectrometer. Interestingly, the FTIR spectra exhibited the evolution processes of CO_3^{2-} and PO_4^{3-} groups over increasing hydrothermal reaction time (Figure 1). The spectrum of the dry cuttlebone was shown in Figure 1a, in which the peaks of 710(s), 856(s), 1083(w), 1400−1650, 1789(w), 2527(w), and 2923(w) cm^{-1} resulted from the presence of a CO_3 group. The wide shoulder peak of 3429 cm^{-1} was assigned to the OH^- group. After 3 h of hydrothermal transformation, the strong absorption peaks of 567, 602, and 1042 cm^{-1} could be distinctly observed in Figure 1b, which were assigned to the characteristic absorption peaks of the PO_4^{3-} tetrahedral groups; all the absorption peaks of CO_3^{2-} groups had large descents. Upon prolonging hydrothermal reaction time (6−48h), the peaks of 856 and 1410 cm^{-1} gradually became to be weak, and the peaks of 2923, 2527, 1789, and 710 cm^{-1} for CO_3^{2-} groups disappeared from the spectra. The FTIR spectra in Figure 1 show evidence of bone-like AB mixed type carbonated apatites,

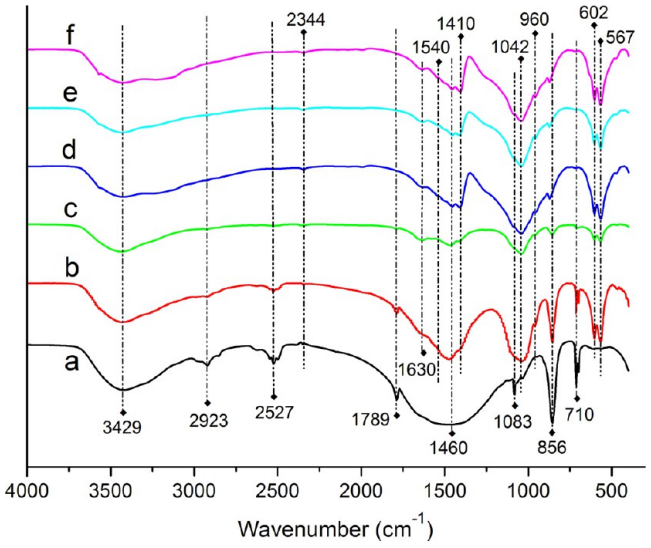

Figure 1. FTIR spectra of treated cuttlebone (a) and the scaffold transformed from hydrothermal reaction at 180 °C for 3 h (b), 6 h (c), 12 h (d), 24 h (e), and 48 h (f).

$Ca_{10}[(PO_4)_{6-x}(CO_3)_x][(OH)_{2-y}(CO_3)_y]$.[28] Previous studies have assigned the peaks at 870, 1430, and 1450 cm^{-1} to B-type and those centered at 880 and 1540 cm^{-1} to A-type.[29] Other studies have assigned the bands centered at 1450, 1540, and 1630 cm^{-1} as evidence of AB mixed type carbonated apatite. Therefore, it has indicated that PO_4 groups could be incorporated into the calcium carbonates lattices during the hydrothermal reaction process partially replacing CO_3 or OH sites forming AB type carbonated apatite. Accordingly, the prepared scaffolds should perfectly match the bone implantation application, since the complex type carbonated apatite may make for the realization of the balance between absorption and degradation in the experiments.

X-ray Diffraction Analyses (XRD). The power XRD analyses have been carried out to confirm the homogeneity of the prodcuts prepared under the hydrothermal reactions (Figure 2). The XRD results showed that the diffraction feature peaks of the dry cuttlebones were consistent with the ones of aragonites (ICDD card 01-071-2396) (Figure 2a,b). The peaks of hydroxyapatite (ICDD card 00-009-0432) were found in the XRD patterns of the products from the hydrothermal reaction for 3−24 h (Figure 2d−g). Two peaks of 16.6 and 23.7° resulted from $(NH_4)_2HPO_4$, exhibiting that a few biphosphammites also inhabited $CaCO_3$ sites in the lattices. All the X-ray spectra obtained for hydrothermal transformation longer than 3 h were similar in terms of the identified phases, indicating that 3 h of the transformation reaction was enough to obtain relative pure hydroxyapatites by the fast reaction kinetics. The phase composition of the scaffolds prepared could also be supported by FTIR spectroscopy.

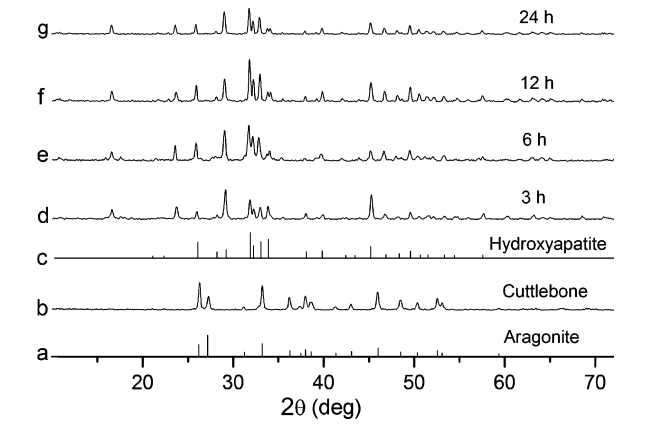

Figure 2. XRD patterns. Aragonite (ICDD card 01-071-2396) (a), cuttlebone (b), hydroxyapatite (ICDD card 00-009-0432) (c), and hydrothermal reaction for 3 h (d), 6 h (e), 12 h (f), and 24 h (g).

Thermogravimetric/Differential Thermal Analyses (TG-DTA). TG-DTA were performed on a Seiko EXSTAR 6300 thermal analyzer with heating and cooling rates of 10 °C/min from room temperature to 1000 °C under a flow of nitrogen. TG curves show that cuttlebones lose the 5 wt % over 30−150 °C corresponding to a lower amount of water, further lose the 8 wt % over 150−500 °C corresponding to an amount of organic matter, and start decomposition of $CaCO_3$ at about 700 °C; final decomposition products should be CaO over 700−850 °C (Figure 3a). Differential thermal analyses (DTA) show two moderate exothermic peaks at 305 and 456 °C (assigned to the combustion of organic matter) and a strong endothermic peak at 832 °C (assigned to a phase change of the decomposition reaction), respectively. Scaffold materials transformed from cuttlebones hardly lose the weight over all temperature ranges of 30−1000 °C but lose a less amount of 2.50 wt %, indicating that most of $CaCO_3$ in cuttlebones has transformed into hydroxyapatites in the hydrothermal reactions. The weight loss of 1.00 wt % in the range of 625−718 °C corresponds to the weight loss of $CaCO_3$ into CaO (Figure 3b). As is known, only part of the internal $CaCO_3$ in the materials may change into CaO for a short heating time.

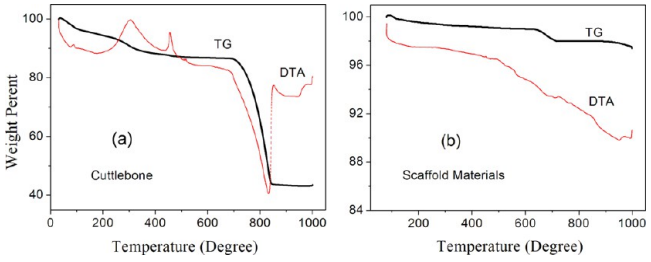

Figure 3. TG-DTA curves. (a) Cuttlebones; (b) scaffold materials transformed from cuttlebones by hydrothermal reactions.

Microstructure Characterization. Scanning electron microscopy (SEM) shows the tunnel-like microstructures of cuttlebones with the trabeculars in the holes (Figure S2a, Supporting Information); the trabeculars consist of the thin layer cutins that enhance mechanical strength of the frameworks. The frameworks of cuttlebones start to collapse into the powder at about 450 °C, and its color changes into black from white due to the organic matter carbonization when sintering. After the hydrothermal reaction, some trabeculares were broken in the unsintered scaffolds (Figure S2b, Supporting Information). The scaffold materials transformed from the cuttlebones by hydrothermal reaction can endure heating over 1000 °C and keep the ordered natural framework, indicating that most of the $CaCO_3$ components have been transformed into HA and/or TCP. The color of the scaffold materials finally changes into bright-white with sintering at 950 °C for 30 min, because all the organic matter changes into volatilizable CO_2 and drops out.

dx.doi.org/10.1021/am400779e | ACS Appl. Mater. Interfaces 2013, 5, 5557−5562

However, the trabeculars in the holes disappeared after high temperature sintering (Figure 4a). The framework of the

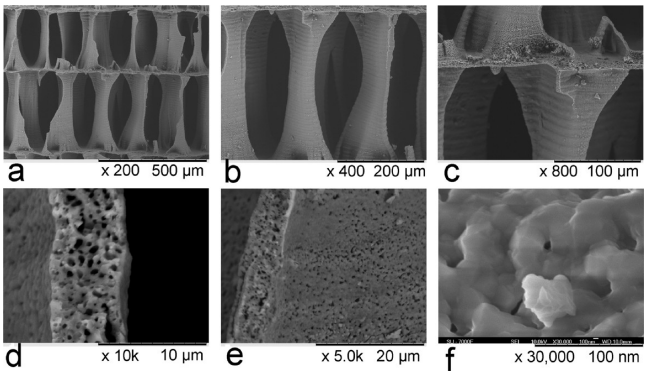

Figure 4. (a) Scanning microscope view of the sintered scaffold transformed from the cuttlebone by hydrothermal reaction, and all the trabeculares were broken in the holes; (b) original magnification of 400× clearly reveals the ordered macroporous framework supported by the S-shaped pillars; (c) the floor supported by the "S" oriented walls; (d) transverse section view of the magnification of 10 000× of the floor with 2−5 μm openings; (e) image of exterior surface of the floor wall; (f) view of the magnification of 30 000× for the ceramic floor.

scaffold is made up of well-organized parallel interlayers and "S" shaped walls, in which the parallel interlayers are supported by "S" oriented walls with 300 μm in height. The distance between neighboring "S" walls is about 100 μm, and dimensional size of the pear-like hole (100 × 200 μm) is suitable for blood circulation and bone cells to plant, conglutinate, and proliferate (Figure 4b). The interlayer can be named as a floor, the thickness of which is about 5−7 μm (Figure 4c). Transverse section and exterior surface of the floor unevenly distribute various small openings with size 2−5 μm (Figure 4d,e). These small openings could promote the microcirculation of the nutrient solutions or induce the germination of the bone cells. Figure 4f shows the ceramic texture of scaffold materials, which has fine biomechanics intensity and provides the appropriate sustentation. From the top-view direction of the scaffold, the tortuous strips correspond to the "S" oriented walls supporting the parallel floors between neighboring layers (Figure 5a). Figure 5b displays the top features of the "S" oriented walls, of which the top surface consists of the nanocrystallites (Figure 5c).[30,31]

Mechanical Properties. The mechanical strengths of the scaffolds were evaluated via testing the materials' compressive and tensile properties using an INSTRON 5966 Tester. For the compressive test, the scaffolds were cut into small cylinders obtained from different sites along horizontal and vertical

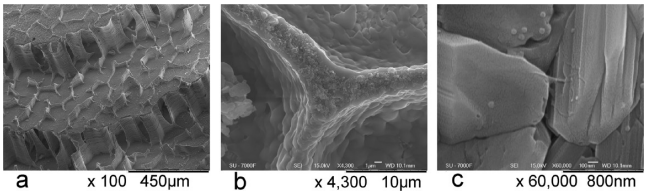

Figure 5. (a) Top view of the scaffold; (b) the top view of the "S" oriented wall; (c) the nanocrystallite composites at the top fracture surface of the "S" oriented walls.

directions, respectively. For the tensile test, the scaffolds were made into small slices. The average value of the tensile strength along the horizontal direction was only 0.0259 MPa (Table 1).

Table 1. Summary of the Tensile Properties of the Scaffolds

entry	strength (MPa)	modulus (MPa)
1	0.0255	48.76
2	0.0263	31.34
average	0.0259	40.05

The compressive strengths in the horizontal direction were far higher than ones in the vertical direction (Table 2). The results

Table 2. Summary of the Compressive Properties of the Scaffolds

	horizontal		vertical	
entry	strength (MPa)	modulus (MPa)	strength (MPa)	modulus (MPa)
1	0.927	102.16	0.175	22.06
2	1.126	87.85	0.221	19.43
3	1.399	97.55	0.259	17.85
average	1.151	95.85	0.218	19.78

above showed the obvious mechanical anisotropic properties of the scaffolds in the different directions with the fine compressive strength and the poor tensile strength in the horizontal direction (details in Figures S3−5, Supporting Information).

In Vitro Anticoagulation Properties. In this work, APTT, PT, and TT were measured to evaluate the anticoagulation effect of the prepared scaffolds. The APTT detects the intrinsic coagulation; PT reveals the extrinsic pathway of the blood-clotting system, and the TT test is performed as the assay for the last step of coagulation, i.e., the thrombin-mediated fibrin formation. Thus, APTT, PT, and TT of blood plasma are commonly carried out to assess the in vitro anticoagulation properties of different biomaterials.[32,33] Table 3

Table 3. APTT, PT, and TT of Scaffolds (Soaking Time = 1 h)

samples	APTT (s)	PT (s)	TT (s)
blood plasma	32.8 ± 3.6	10.6 ± 1.8	12.7 ± 1.8
scaffolds	32.8 ± 4.7	10.5 ± 0.3	13.4 ± 2.3

showed the effects of the scaffolds on APTT, PT, and TT of human blood plasma. The values of APTT, PT, and TT of human blood plasma were 32.8 ± 3.6, 10.6 ± 1.8, and 12.7 ± 1.8, respectively. There was no significant difference between the data of blood plasma incubated with the prepared scaffolds and those of human blood plasma ($P > 0.05$), apart from the average of TT being slightly prolonged from 12.7 ± 1.8 for human blood plasma to 13.4 ± 2.3.

Cytotoxicity Test. Optical absorbency (OD) values were measured by the enzyme mark instrument at 490 nm, and the viabilities were calculated by the eq 1. Table 5 showed the cytotoxicity test results of the samples. According to Table 4, the cytotoxicity of the 100% extracts of the scaffold was in the level 0, having a relatively higher degree of proliferation and not much difference compared with the values of the negative control group ($P > 0.05$), which revealed that the test sample

dx.doi.org/10.1021/am400779e | ACS Appl. Mater. Interfaces 2013, 5, 5557−5562

Table 4. Evaluation Form of Cytotoxic Effects (%)

grades	relative viability
0	≥100
1	75−99
2	50−74
3	25−49
4	1−24

Table 5. Cytotoxicity of Scaffolds Evaluated by MTT Assay

projects	consistency (%)	absorbency ($\bar{x} \pm s$)	viability (%)
extracts of scaffolds	100	0.554 ± 0.015	107.4
phenol solution	1	0.490 ± 0.020	95.0
	10	0.250 ± 0.046	48.4
	15	0.031 ± 0.016	6.0
	25	0.003 ± 0.003	0.6
extracts of polyethylene		0.516 ± 0.034	100.0

had no inhibitory effect on the cell proliferation. That is to say it is nontoxic for the 100% extracts of the sample. For positive control groups, the extracts of 1% were noncytotoxic; the others all have significant toxic effects.

$$\text{viab. } \% = (100 \times \text{OD}_t)/\text{OD}_n \quad (1)$$

Here, OD_t was the mean value of the measured optical density of the test samples; OD_n was the mean value of the measured optical density of the negative groups. The eq 1 was used to calculate the reduction of viability compared to the negative groups.[32,33]

Experiments in Vitro and Vivo. Cell proliferation and adhesion experiments were carried out. Adv-GFP-labeled hMSCs were seeded in the scaffolds and cultured for different times. A great number of Adv-GFP-labeled hMSCs with green fluorescence were clearly observed on the surfaces of the scaffold materials under a fluorescent microscope (Figure S6, Supporting Information), indicating that the prepared materials as bone tissue engineering scaffolds or fillers have fine biocompatibility suitable for adhesion and proliferation of the hMSCs.

Experimental in vitro was shown in Figure 6; after hMSCs were inoculated on the surface of the scaffolds for 2 d, the

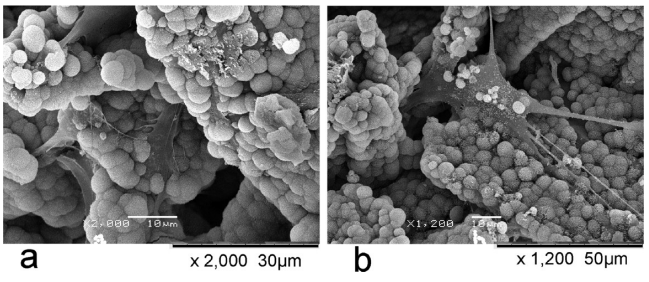

Figure 6. SEM images of the proliferation and adhesion on the scaffold surfaces: (a) cell inoculation for 2 d and (b) 6 d.

survived cells were observed clearly. The cells extended out pseudopod-like structures adhered to the material surfaces, which indicated the cells could commendably adapt to the surface morphology of the materials (Figure 6a). After being inoculated for 6 d, the cells extended more significantly and grew into the pores gradually; the secretory granules from the metabolic activity and rough cord-like collagen fibers on the cell surfaces were observed (Figure 6b), which further confirmed that the scaffolds had the fine biocompatibility.

Histological analyses (experiment in vivo) were carried out by implanting the scaffolds stained with eosin into rabbit femur. Two weeks after the implantation of the scaffolds, many small bone precursor cells with vague shapes were observed on the material surface (Figure 7a). Four weeks after the operation,

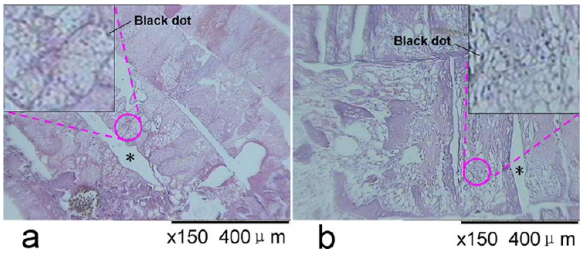

Figure 7. Histological view of the specimens in vivo. (a) Two weeks; (b) four weeks. Sections were stained with eosin. Asterisks (*) represented the implanted scaffolds. Black dots represented the bone cells.

the bone cells grew into bigger ones (Figure 7b, black dots). The bioabsorption of the scaffolds and replacement by newly formed bone tissues were slowly performed along with the formation and infiltration of the osteoblasts.

4. CONCLUSIONS

In conclusion, the results of this study suggested that the scaffold materials for bone reconstruction could be transformed from cuttlebones by the hydrothermal reaction. The prepared materials kept the initial ordered macroporous structures nontoxic as evaluated by the MTT test. Experiments in vitro and vivo showed that the scaffolds had fine biocompatibility and were favorable to the adhesion and growth of the cells, the osteogenic differentiation of stem cells. In the follow-up works, the authors would perform further research about biocompatibility, biodegradation, bioactivity in the body, and the application feasibility of the materials for the bone tissue engineering scaffolds or graft substitutes.

■ ASSOCIATED CONTENT

Ⓢ Supporting Information

Experimental details and characterization data. This material is available free of charge via the Internet at http://pubs.acs.org.

■ AUTHOR INFORMATION

Corresponding Author

*Tel.: +86-574-87600869. E-mail: lixing@nbu.edu.cn.

Notes

The authors declare no competing financial interest.

■ ACKNOWLEDGMENTS

The work was supported by the National Natural Science Foundation of China (20971075, 81273130), the NSF of Zhejiang province (LY12B01005, LY12C20004), Ningbo Municipal Natural Science Foundation (2010A610060, 2010C500009, 2012A610223, 2012C50001), the Ningbo Programs for Innovative Research Team (2009B21007, 2011B82014), and the K. C. Wong Magna Fund in Ningbo University.

REFERENCES

(1) Bhumiratana, S.; Grayson, W. L.; Castaneda, A.; Rockwood, D. N.; Gil, E. S.; Kaplan, D. L.; Vunjak-Novakovic, G. *Biomaterials* **2011**, *32*, 2812−2820.
(2) Jeong, C. G.; Hollister, S. J. *Biomaterials* **2010**, *31*, 4304−4312.
(3) Hoshino, M.; Egi, T.; Terai, H.; Namikawa, T.; Takaoka, K. *Biomaterials* **2006**, *27*, 4934−4940.
(4) Stevens, M. M.; George, J. H. *Science* **2005**, *310*, 1135−1138.
(5) Lutolf, M. P.; Gilbert, P. M.; Blau, H. M. *Nature* **2009**, *462*, 433−441.
(6) Lu, H. X.; Hoshiba, T.; Kawazoe, N.; Chen, G. P. *Biomaterials* **2011**, *32*, 2489−2499.
(7) Bauer, T. W. *Skeletal Radiol.* **2007**, *36*, 1105−1107.
(8) Zhang, X.; Awad, H. A.; O'Keefe, R. J.; Orthop, Clin. *Relat. Res.* **2008**, *466*, 1777−1787.
(9) Tomford, W. W. *J. Bone Joint Surg. Am.* **1995**, *77*, 1742−1754.
(10) Babensee, J. E.; Anderson, J. M.; McIntire, L. V.; Mikos, A. G. *Adv. Drug Delivery Rev.* **1998**, *33*, 111−139.
(11) Bakos, D.; Soldan, M.; Fuentes, I. H. *Biomaterials* **1999**, *20*, 191−195.
(12) Murphy, W. L.; Kohn, D. H.; Mooney, D. J. *J. Biomed. Mater. Res., Part A* **2000**, *50*, 50−58.
(13) Liao, S.; Cui, F.; Zhang, W.; Feng, Q. *J. Biomed. Mater. Res., Part B* **2004**, *69*, 158−165.
(14) Chai, C.; Leong, K. W. *Mol. Ther.* **2007**, *15*, 467−480.
(15) Zhao, H. X.; Dong, W. J.; Zheng, Y. Y.; Liu, A. P.; Yao, J. M.; Li, C. R.; Tang, W. H.; Chen, B. Y.; Wang, G.; Shi, Z. *Biomaterials* **2011**, *32*, 5837−5846.
(16) Dong, W.; Zhang, T.; Epstein, J.; Cooney, L.; Wang, H.; Li, Y. *Chem. Mater.* **2007**, *19*, 4454−4459.
(17) Zheng, L. Q.; Yang, F.; Shen, H.; Hu, X. F.; Mochizuki, C.; Sato, M.; Wang, S. G.; Zhang, Y. D. *Biomaterials* **2011**, *32*, 7053−7059.
(18) Soballe, K. *Acta Orthop. Scand. Suppl.* **1993**, *255*, 1−58.
(19) Kothapalli, C. R.; Shaw, M. T.; Wei, M. *Acta Biomater.* **2005**, *1*, 653−662.
(20) Brandt, J.; Henning, S.; Michler, G.; Schulz, M.; Bernstein, A.; Schulz, M. *J. Mater. Sci. Mater. Med.* **2010**, *21*, 283−294.
(21) Zhang, Y.; Zhang, M. *J. Biomed. Mater. Res., Part A* **2002**, *61*, 1−8.
(22) Culverwell, E.; Wimbush, S. C.; Hall, S. R. *Chem. Commun.* **2008**, 1055−1057.
(23) Li, Y. P.; Li, X.; Peng, Z. X.; Xu, H. P.; Bing, Y.; Xu, L. P.; Tang, H. L.; Dong, P.; Zhuang, H. M. *J. Tradit. Chin. Orthop. Traumatol.* **2010**, *22*, 3−7.
(24) Liu, H. F.; Li, X. M.; Niu, X. F.; Zhou, G.; Li, P.; Fan, Y. B. *Biomacromolecules* **2011**, *12*, 2914−2924.
(25) Meng, S.; Zhong, W.; Chou, L.S. L.; Wang, Q. H.; Liu, Z. J.; Du, Q. G. J. *Appl. Polym. Sci.* **2007**, *103*, 989−997.
(26) Espuelas, S.; Legrand, P.; Irache, J. M.; Gamazo, C.; Orecchioni, A. M.; Devissaguet, J. P.; Ygartua, P. *Int. J. Pharm.* **1997**, *158*, 19−27.
(27) Kim, S. Y.; Lee, Y. M.; Shin, H. J.; Kang, J. S. *Biomaterials* **2001**, *22*, 2049−2056.
(28) Rocha, J. H. G.; Lemos, A. F.; Kannan, S.; Agathopoulos, S.; Ferreira, J. M. F. *J. Mater. Chem.* **2005**, *15*, 5007−5011.
(29) Landi, E.; Celloti, G.; Logroscino, G.; Tampieri, A. *J. Eur. Ceram. Soc.* **2003**, *23*, 2931−2937.
(30) Nejati, E.; Firouzdor, V.; Eslaminejad, M. B.; Bagherii, F. *Mater. Sci. Eng., C* **2009**, *29*, 942−949.
(31) Zaremba, C. M.; Morse, D. E.; Mann, S.; Hansma, P. K.; Stucky, G. D. *Chem. Mater.* **1998**, *10*, 3813−3824.
(32) Wu, L. X.; Guo, Z.; Meng, S.; Zhong, W.; Du, Q.; Chou, L. L. *Appl. Mater. Interfaces* **2010**, *2*, 2781−2788.
(33) Guo, Z.; Meng, S.; Zhong, W.; Du, Q.; Chou, L. L. *Appl. Surf. Sci.* **2009**, *255*, 6771−6780.